

RESEARCH ARTICLE

Automated Segmentation of Skin Strata in Reflectance Confocal Microscopy Depth Stacks

Samuel C. Hames¹, Marco Ardigo², H. Peter Soyer¹, Andrew P. Bradley³, Tari W. Prow^{1*}

1 Dermatology Research Centre, The University of Queensland, School of Medicine, Translational Research Institute, Brisbane, Australia, **2** San Gallicano Dermatological Institute—IRCCS, Rome, Italy, **3** The University of Queensland, School of Information Technology and Electrical Engineering, Brisbane, Australia

* t.prow@uq.edu.au



OPEN ACCESS

Citation: Hames SC, Ardigo M, Soyer HP, Bradley AP, Prow TW (2016) Automated Segmentation of Skin Strata in Reflectance Confocal Microscopy Depth Stacks. PLoS ONE 11(4): e0153208. doi:10.1371/journal.pone.0153208

Editor: Konradin Metze, University of Campinas, BRAZIL

Received: May 12, 2015

Accepted: March 25, 2016

Published: April 18, 2016

Copyright: © 2016 Hames et al. This is an open access article distributed under the terms of the [Creative Commons Attribution License](https://creativecommons.org/licenses/by/4.0/), which permits unrestricted use, distribution, and reproduction in any medium, provided the original author and source are credited.

Data Availability Statement: The RCM image data is available from the Dryad repository (doi:[10.5061/dryad.rg58m](https://doi.org/10.5061/dryad.rg58m)).

Funding: This work was supported by Cancer Council Queensland (www.cancerqld.org.au) through grant APP1058641. The funders had no role in study design, data collection and analysis, decision to publish, or preparation of the manuscript.

Competing Interests: The authors have read the journal's policy and have the following competing interests: Peter Soyer is a shareholder in and provides regular tele-dermatological reports for e-

Abstract

Reflectance confocal microscopy (RCM) is a powerful tool for *in-vivo* examination of a variety of skin diseases. However, current use of RCM depends on qualitative examination by a human expert to look for specific features in the different strata of the skin. Developing approaches to quantify features in RCM imagery requires an automated understanding of what anatomical strata is present in a given en-face section. This work presents an automated approach using a bag of features approach to represent en-face sections and a logistic regression classifier to classify sections into one of four classes (stratum corneum, viable epidermis, dermal-epidermal junction and papillary dermis). This approach was developed and tested using a dataset of 308 depth stacks from 54 volunteers in two age groups (20–30 and 50–70 years of age). The classification accuracy on the test set was 85.6%. The mean absolute error in determining the interface depth for each of the stratum corneum/viable epidermis, viable epidermis/dermal-epidermal junction and dermal-epidermal junction/papillary dermis interfaces were 3.1 μm , 6.0 μm and 5.5 μm respectively. The probabilities predicted by the classifier in the test set showed that the classifier learned an effective model of the anatomy of human skin.

Introduction

Reflectance confocal microscopy (RCM) is capable of imaging human skin *in-vivo* at high resolution, with available machines capable of lateral resolutions of 0.5–1 μm [1]. RCM has been established as an effective tool for many applications in the assessment of human skin, such as the diagnosis of melanoma and keratinocyte skin cancers [2,3] and the assessment of inflammatory skin diseases [4]. However, appropriate training and experience are required to interpret RCM imagery: unlike the transverse sections of histopathology RCM images are acquired en-face and instead of the contrast provided by hematoxylin and eosin staining only a monochrome image showing variation in reflectance at one wavelength is available. While the non-invasive character of RCM imaging allows for the collection of large numbers of images,

derm consult GmbH and MoleMap by Dermatologists Pty Ltd. This does not alter the authors' adherence to PLOS ONE policies on sharing data and materials. The remaining authors have declared that no competing interests exist.

extracting quantitative information requires the time and expense of evaluation by a human expert. Fully exploiting the potential of RCM as a non-invasive imaging source requires new tools for standardised and streamlined assessment of large datasets.

While several approaches to standardised assessment using image analysis have been proposed none are currently in clinical use. These assessment approaches have focused on one of three main categories: 1) Quantifying and detecting specific features such as counting keratinocytes [5], detecting pagetoid cells [6] and evaluating photoageing [7], 2) Computer aided diagnosis of malignant melanocytic lesions [8] and 3) Identifying the anatomical structures of human skin [9,10]. Although both Somoza et al. and Kurugol et al. considered the problem of understanding human skin their work is limited: Kurugol et al. consider only the location of the dermal-epidermal junction and showed good performance only in darker skin types: 89% of the epidermis and 87% of the dermis were correctly classified in dark skin, whereas in light skin only 64% and 75% of the epidermis and dermis were correctly classified. The transition layer between the two was accurately classified only 41% of the time in light skin. While Somoza et al. showed an approach for complete segmentation of human skin their results were only a pilot study on 3 stacks. To date there is no robust automated method for understanding the complete anatomical structure of human skin in RCM depth stacks.

Understanding the anatomical structure of the skin is one of the fundamental tasks for assessment of RCM and conventional histopathology. It is necessary firstly for examining gross changes, such as thickening of the viable epidermis or stratum corneum. Secondly, an understanding of the distinct strata is also needed to guide the search for specific features. For example examining the honeycomb pattern of keratinocytes in the viable epidermis as a feature of photoageing [11] requires knowing at what depth the viable epidermis occurs in a stack. Therefore automated segmentation of the anatomical strata of the skin is a valuable starting point for standardised and automated analysis of RCM depth stacks.

The aim of this study was to develop a tool for automatically segmenting the distinct anatomical strata of human skin. This paper will outline an approach for achieving this aim using a bag of features approach to representing en-face optical sections that uses a dictionary of visual features learned by clustering image patches extracted from en-face RCM sections. The Supporting Information section contains the individual data from the analysis (S1–S4 Tables). A schematic representation describing the algorithm is included in S1 Fig. The segmentation code is contained in the S1 Archive. This approach was trained and validated by comparison with an expert human observer. A bag of features approach was selected because these models are capable of modelling textural features and make minimal assumptions about the nature of the problem. In addition the representative features are learned directly from the image data and do not require manual selection of relevant features. Bag of features also have demonstrated success in a number of medical imaging applications including, for example, colorectal tumor classification in endoscopic images [12], X-ray categorization [13] and histopathology image classification [14].

Methods

Participants and data acquisition

This study was conducted according to the Declaration of Helsinki with approval from the Metro South Human Research Ethics Committee and written informed consent obtained from participants. Participants were recruited in two age groups to represent a spectrum of normal skin. A total of 57 participants were recruited: 25 aged 20–30 (14 female) and 32 aged 50–70 (18 female). For the 20–30 year old group there were 7 phototype I, 9 phototype II, 7 phototype III, 1 phototype IV and 1 with no data available. For the 50–70 year old group there were 9

phototype I, 9 phototype II, 12 phototype III, 1 phototype IV and 1 with no data available. Recruitment focused on phototypes I-III to study photoageing in the context of light skin types. This dataset thus forms an ideal testbed for algorithm development in the context of the most challenging phototypes to examine with RCM. This dataset forms a superset of the data from Australian participants examined for the signs of photoageing in [11] and also used in [7].

Dorsal and volar skin of the forearm was imaged using a Vivascope 1500 (Caliber I.D, Rochester, NY, USA). A depth stack of en-face optical sections with vertical spacing of $2\ \mu\text{m}$ was acquired to a depth of at least 50 sections ($100\ \mu\text{m}$). Each en-face section had a field of $500\ \mu\text{m}$ by $500\ \mu\text{m}$ and 1000 by 1000 pixels. At least 2 stacks were acquired for each participant and body site, leading to a dataset of 335 stacks.

Strata definition and labelling

For the purposes of segmentation four distinct anatomical strata were identified in the skin: the stratum corneum, viable epidermis, dermal-epidermal junction and the papillary dermis. To simplify the problem of establishing a ground truth in a large number of stacks it was assumed that a single anatomical strata was present in each en-face section and the extent of each strata was determined by identifying where three distinct features first occurred within the stack, as illustrated in Fig 1. This approach was inspired by work on weakly supervised video

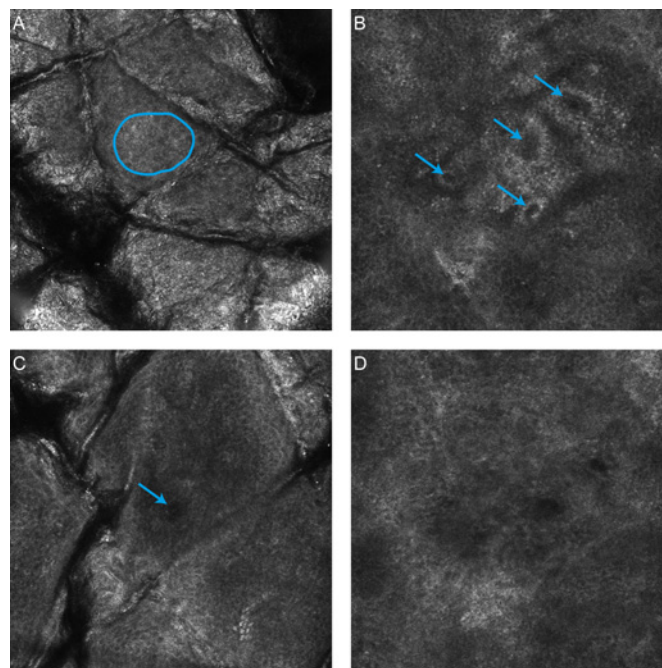


Fig 1. RCM features used in identification of the start and end of each anatomical strata. A) The start of the viable epidermis is marked by the first visible honeycomb pattern (Blue outline). B) The start of the dermal-epidermal junction is marked by the first clearly defined papillae with bright ring of basal cells surrounding a dark centre (Blue arrows). C) The start of the papillary dermis is marked by the absence of features corresponding to the basal layer. D) Alternative definition of the start of the dermal-epidermal junction for light skin types, a dark featureless patch surrounded by keratinocytes with the absence of a bright basal layer (Blue arrow).

doi:10.1371/journal.pone.0153208.g001

classification [15]. The specific features were based on [16]: visible honeycomb patterns corresponding to viable keratinocytes, visible bright bands corresponding to basal cells/dermal papillae and finally the absence of features of the basal layer -or- clearly visible fibrillar structures in the dermis. The en-face section with the first visible honeycomb pattern was considered the first layer of the viable epidermis—all sections above this layer were labelled as stratum corneum. En-face sections from the first honeycomb pattern to the first dermal papillae were labelled as viable epidermis. Sections from the first dermal papillae and up to, but not including, the en-face section where the features of the basal layer were no longer visible were labelled as dermal-epidermal junction. All sections below these were labelled as papillary dermis.

The dataset was labelled by a dermatologist with significant clinical experience with RCM (MA). Labelling was performed twice with four weeks in between to assess the intra-observer variability of the selected features. This second labelling was taken to be the ground truth for evaluation purposes due to the improved familiarity with the specific features and confidence in the results by the assessor. Stacks were organised by participant and body site and were labelled sequentially as would be performed in a clinical setting.

Some stacks showed motion or other artefacts making accurate labelling impossible—these stacks were excluded from the analysis. In addition if fewer than two examples for each body site were considered acceptable a participant was excluded from the analysis. A total of 16,144 images in 308 stacks from 54 participants could be successfully labelled and were included for further analysis.

The complete set of labelled RCM sections in a form suitable for automated analysis is made available in [17].

Representation of en-face sections using bags of features

A dictionary of representative visual features was learned using a process adapted from [18] using normalisation, whitening and spherical k-means to cluster small image patches drawn from the set of stacks. Initially the original high resolution optical sections were down-sampled by a factor of 4 in each direction to 250 by 250 pixels ($2\ \mu\text{m}$ per pixel). A truncated sinc pre-filter was used to limit aliasing. This was necessary to match the scale of the extracted patches to the expected features in the image, and also to limit the dimensionality of features used in clustering. Following resizing a fixed number of patches were extracted from random locations in each en-face section. These patches were normalised to zero mean and unit variance (regularised by a constant to avoid singularities for low variance patches). These normalised patches were then whitened using a whitening matrix learned from the all extracted patches using the zero component analysis (ZCA) transform. Following [18] a regularisation factor, ϵ , was used, and additionally, only the top eigenvectors such that 95% of the energy was preserved in the transform were retained [19]. This last step was necessary to avoid numerical instability due to a number of low energy principle axes. After whitening the dictionary was learned by clustering using spherical k-means [20]. For encoding and clustering speed a hierarchical approach was applied to clustering, after [21,22]. A fixed number of iterations were used at each layer in the hierarchy, both for simplicity, and because of previous observations that few iterations are necessary for convergence [18].

Having learned a dictionary, each en-face section was then represented by the histogram of counts of visual features found in the image. Initially all raw patches in an en-face section were extracted in a dense sliding window fashion. The extracted patches were normalised using the same regularisation process as previous and then whitened using the whitening matrix found while learning the dictionary. A whitened patch was quantized to the most similar (in a cosine

sense) element in the dictionary. The final histogram was term-frequency normalised to be of unit length (L2 norm).

An augmentation approach was used to expand the dataset for training and testing and to reduce the rotation variance of the algorithm: each en-face section was considered along with three rotations (at 90, 180 and 270 degrees). In other words each section, plus the three rotations of that section were encoded separately. In the training phase these rotated examples plus the original section were considered as separate en-face sections while at testing phase the histograms from each rotation were pooled by averaging. This augmentation is analogous to an approach commonly used in deep learning and convolutional neural networks where the dataset is expanded by symmetry transformations and translations (for example [23]).

The histograms of visual feature counts for each en-face section were finally classified using L1 regularised logistic regression from the scikit-learn package [24]. The multiple classes were handled using a one-vs-rest scheme. Logistic regression was selected as a classifier because it can output meaningful probability estimates. L1 regularisation was selected for its demonstrated performance in handling cases with large number of irrelevant features [25], as might be expected to occur when learning a large number of features using a simple clustering methodology.

Additional detail about this method is contained in [26], and the complete implementation and computational pipeline is included in [S1 Archive](#).

Parameter estimation and performance assessment

A stratified random sample of participants from the two age groups (18 of the 54 participants, 8 from the 20–30 age group, 10 from the 50–70 age group) was held out as a final test set. The remainder were used for training and parameter estimation. Ten fold cross validation partitioned on the participants was then used on the training set with a coarse grid search to determine the parameters for maximum mean classifier accuracy over all of the folds. The grid search investigated the number of layers (1–3) and the number of splits at each layer (4–18) in the hierarchical dictionary as well as the logistic regression regularisation constant C (10^0 , 10^1 , \dots , 10^5). The number of splits and number of levels in the representation as well as the total number of patches extracted for the dictionary learning process were constrained so that the dictionary learning process and the classifier training process could be performed comfortably on a machine with 16GB of RAM. Other parameters were held constant: the size of extracted patches (7x7 pixels), the regularisation parameters for the patch normalisation (1—smaller than recommended by [18] to avoid changing the contrast too much for patches that do not require normalisation) and the whitening transform (0.1—as recommended for 8x8 pixel patches by [18]), the energy retained in the ZCA transform (95%) and the number of iterations of the spherical k-means algorithm (10—as discussed earlier).

The classification performance of the algorithm was measured by applying the dictionary learning, encoding and classifier training process to the complete training set (with the optimal parameters selected by the grid search), then applying the learned feature encoding and classifier to the test set. The test set was not used at any point for training, validation or tuning. The output of the multi-class classifier was assessed by calculating the accuracy over all classes and the confusion matrix between the dermatologist labelling and the automatic classifications. The accuracy was also calculated for combinations of age and body site with strata type or phototype. To ensure that the classification was reliable for all stacks and not just on average the accuracy of the classifier was also calculated per stack in the test set.

Clinical utility was further assessed by using the classification output to estimate the interface locations between each strata. Each interface location was determined by counting the

Table 1. Comparison of human intraobserver agreement with automated approach on the 5319 sections in the test set.

	Dermatologist (1st Label)				Automatic				
	SC	VE	DEJ	PD	SC	VE	DEJ	PD	
Dermatologist (2nd Label)	SC	1292	1	0	0	1209	58	3	23
	VE	23	1285	9	0	71	1085	154	7
	DEJ	0	56	1523	22	0	143	1298	160
	PD	0	0	26	1082	3	0	143	962

Key: SC = Stratum Corneum, VE = Viable Epidermis, DEJ = Dermal-epidermal Junction, PD = Papillary Dermis.

doi:10.1371/journal.pone.0153208.t001

number of sections classified as each anatomical strata. This number of layers is converted to a depth by multiplying by the depth between en-face sections. For example, the interface between the viable epidermis and the dermal-epidermal junction would be estimated as the sum of the number of sections classified as stratum corneum and viable epidermis multiplied by the 2 μm vertical section spacing. Agreement between the dermatologist and automatically identified interfaces was measured by calculating the mean absolute error in interface position, as well as the Pearson correlation coefficient between the interface depths.

Results

The classification accuracy over the entire test set was 85.6%. The parameters that optimised classification accuracy were a three layer encoding with 18 splits at each level (5832 total visual features) and C of 100. In comparison the intra-observer agreement of the dermatologist was 97.4%. The confusion matrices showing how images of each anatomical strata were classified by both the dermatologist and the automated method, are shown in [Table 1](#). [Table 2](#) shows the classification accuracies broken down by combinations of age, body site, strata and phototype. The complete classification results for the 5319 en-face sections in the test set are given in [S1 Table](#).

The classification accuracy for each stack, and the agreement between the automatic and dermatologist identified interfaces between strata are shown in [Fig 2](#). The average absolute error and standard deviation in locating all interfaces was 4.8 ± 4.8 μm. The average absolute error and standard deviation of the error in locating each interface was 3.1 ± 3.3 μm, 6.0 ± 5.3 μm and 5.5 ± 5.0 μm for the interfaces between the stratum corneum/viable epidermis, viable

Table 2. Percentage of correctly classified sections by the automated approach in each subgroup.

		Strata				Phototype			
		SC	VE	DEJ	PD	I	II	III	Other
20–30 years	Dorsal	95.7	82.8	88.7	91.2	90.9	84.4	90.0	-
	Volar	91.2	79.7	85.1	62.9	80.2	84.0	80.0	-
50–70 years	Dorsal	91.9	82.2	76.8	92.5	80.3	94.0	84.6	86.0
	Volar	95.6	84.2	77.0	92.6	85.9	88.7	89.3	87.6
Phototype	I	88.8	85.2	79.2	88.4				
	II	95.2	80.6	85.9	87.4				
	III	95.7	83.0	80.6	82.3				
	Other	95.5	77.4	81.0	92.9				

Key: SC = Stratum Corneum, VE = Viable Epidermis, DEJ = Dermal-epidermal Junction, PD = Papillary Dermis.

doi:10.1371/journal.pone.0153208.t002

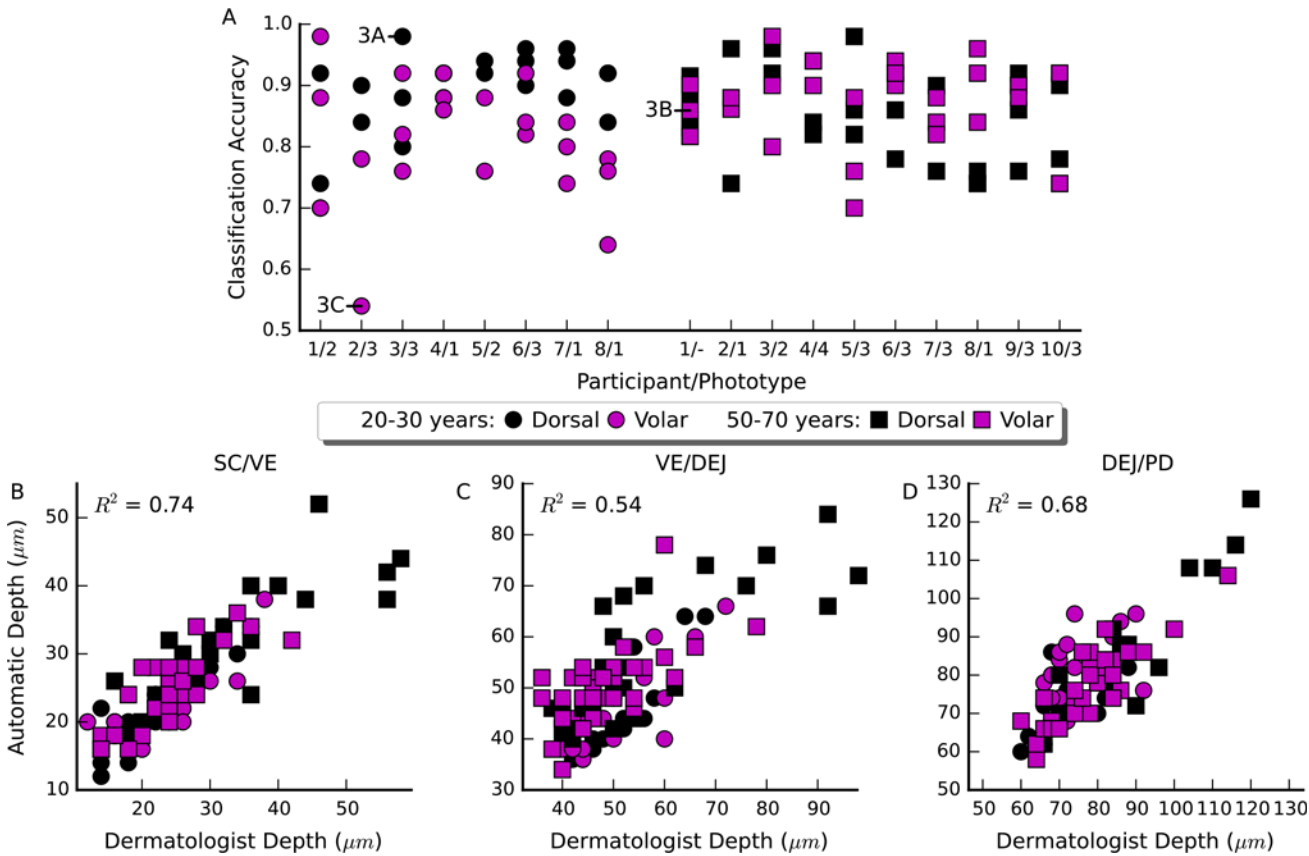


Fig 2. Accuracy and agreement of the automated approach with the dermatologist for individual stacks. A) Classification accuracy across all test stacks, organised by participant. The annotated examples are the best, average and worst accuracy stacks shown in Fig 3. B-D) The correlation between the dermatologist identified interface and the automatically identified interface for each of the stratum corneum/viable epidermis, viable epidermis/dermal-epidermal junction and dermal-epidermal junction/papillary dermis interfaces.

doi:10.1371/journal.pone.0153208.g002

epidermis/dermal-epidermal junction and dermal-epidermal junction/papillary dermis respectively. The complete classification results for each stack in the test set are given in S2 Table.

Examples of automated and dermatologist identified interfaces are shown in Fig 3. Also shown are the estimated strata probabilities through the depth of the stack, as estimated using the logistic regression classifier.

Discussion

The visual features used to localize the anatomical strata within a stack were highly repeatable for the dermatologist observer (97.4% agreement between the first and second labelling sessions). In comparison the automated approach achieves a classification accuracy of 85.6%—a promising result for further automated analysis techniques. In particular the classification accuracy of the stratum corneum was excellent and did not strongly depend on the body site or age of the participant (Table 1). In other strata performance was lower, but there did not appear to be a clear pattern in terms of body site or age. Similarly there did not appear to be a pattern for the classification accuracy of different phototypes. Since for all participants there is at least one stack classified with at least 90% accuracy (Fig 2A), it is likely that the performance depends on some other characteristic of an individual stack. This other characteristic affecting performance could be the implicit assumption that a single strata is present in each en-face

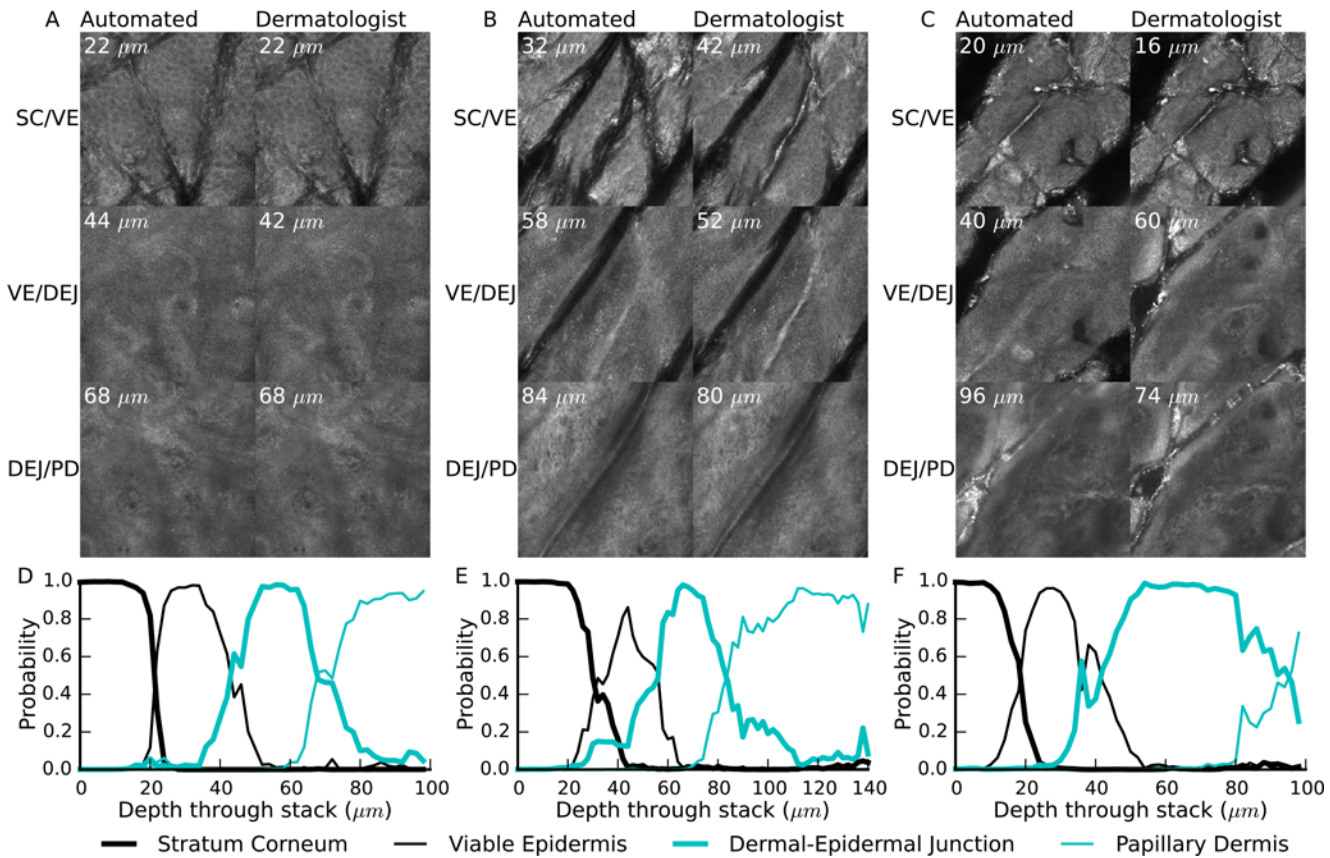


Fig 3. Example interfaces and probability output from the classifier. A-C) Comparison of the dermatologist identified interfaces with the automatically identified interfaces on the stacks with the highest, average and lowest accuracy respectively. D-F) The corresponding probability of each anatomical strata occurring in a section through the depth of the stack.

doi:10.1371/journal.pone.0153208.g003

section: in the least accurately classified stack (Fig 3C) there are furrows extending deep into the stack, causing a mixture of multiple anatomical strata present in each en-face section, whereas the most accurately classified example (Fig 3A) exhibited only superficial furrows and approximately one anatomical strata per section. The stack with average accuracy (Fig 3B) also exhibited deep furrows, but without bright reflectance and without strong mixing of strata.

Interpreting the results of the classification algorithm to identify the depths of different anatomical strata shows good agreement between the dermatologist and automated approach (Fig 2B–2D). The mean absolute error in interface location was less than 6 μm for all three interfaces considered. In other words, on average less than three vertical en-face sections separated the dermatologist identified interface from the automatically identified interface. In the stratum corneum/viable epidermis in particular the average error was only 3.1 μm or just over 1.5 times the vertical depth spacing of en-face sections. Coupling this low absolute error with the high correlation between the dermatologist and automatically identified interface depth (R^2 0.74) suggests a possible use of this method to objectively quantify the thickness of the stratum corneum *in-vivo*.

Beyond the high classification accuracy the utility of this classification approach for further automated analyses is supported by examining the probabilistic output of the logistic regression classifier used (Fig 3D–3F). Despite being trained on individual sections the classifier effectively describes the order and transitions between different strata, with interface regions

showing mixing of probabilities between different strata. Even in the least accurately classified stack, the estimated strata probabilities provide a useful approximate guideline as to where each anatomical strata is located within the stack.

Other work has analysed the structure of RCM depth stacks in different ways. Kurugol et al. [9] segmented the full three dimensional shape of the dermal-epidermal junction based on low-level image features computed on image tiles. Unlike the approach presented here, where whole en-face sections are classified independently as one of the four anatomical strata in the skin, they classify small tiles within each section as either above or below the dermal-epidermal junction and use smoothing both through the depth of the stack and across sections to ensure locally consistent results. In using this spatial information they limit the application of their method to depth stacks alone, but determine a more accurate picture of the shape of the dermal-epidermal junction. It is not clear if their approach would be applicable to mosaics of RCM sections at the same depth, or examples of pathological skin where the layout of the anatomical strata can be disrupted. By not using such spatial information the algorithm outlined in this work can be directly applied to such mosaics, and is expected to perform better in examples of skin that are not normal. While the algorithm presented by Kurugol et al. is capable of delineating a detailed dermal-epidermal junction surface rather than identifying the depth of a single section as reported here, the algorithm in this report is also capable of identifying the other strata of the skin.

Their algorithm was tested on 30 stacks from 30 participants, 15 light skin (phototype I-II) and 15 dark skin (phototype III-VI)—variations in skin appearance with aging and sun exposure were not considered. To analyse light phototypes they attempted to estimate a 'transition' region that approximately contained the dermal-epidermal junction—similar to the volume containing the dermal-epidermal junction reported here. Their results in the light skin stacks are closest to the results presented here (phototype I-III). The average error in identifying the start and end of the volume containing the dermal-epidermal junction in this work (5.5 and 4.8 μm respectively) is broadly comparable to their reported error in identifying the start and end of their transition region (8.3 and 7.6 μm respectively). Also their algorithm could only identify the 41% of the transition volume correctly, whereas this algorithm correctly identified 81.1% of sections from the dermal-epidermal junction. These results suggest that both algorithms are capable of automatically identifying the depth of the dermal-epidermal junction for automating the depth selection of RCM mosaic images (One application suggested by Kurugol et al.). However it should be noted that their algorithm focuses on the more difficult problem of analysing small tiles within a section, rather than identifying whole sections as in this work.

Similar to this work Somoza et al. [10] show a method for classifying en-face sections as a single distinct strata. They define five strata from the stratum corneum to the papillary dermis. To classify en-face sections they use vector quantisation of histograms of visual features. The visual features were derived from a small set of hand selected filters, including oriented derivative of gaussians and laplacian of gaussians. In comparison, this work learns the features from the RCM sections themselves using unsupervised clustering. Although they show promising correlations between human and automated assessment (correlation coefficients 0.84–0.95), they examine only three RCM depth stacks and it is not clear if their work will generalise to other stacks. By comparison this work reports results on a much larger series of stacks and uses a robust validation approach with an independent test set used for final performance evaluation.

The method presented here is limited by three factors. Firstly, only dorsal and volar skin of the forearm is considered. This limitation is mitigated by the inclusion of multiple age-groups and a selection of phototypes, both factors that lead to observable changes in the skin. Secondly the focus is limited to phototypes I-III. However, this limitation is necessary to focus on the

most challenging examples for human observers to examine, and it has already been shown that the improved reflectance of darker skin types are easier to examine automatically [9]. Since the method presented here incorporates brightness and contrast normalisation and focuses on learned features it is reasonable to expect that it will also work with phototypes IV and above. The third limitation is the focus on examples of normal skin. For the best accuracy it would be necessary to train with specific examples of the disease pathology. However many skin diseases, such as inflammatory diseases, present as pathological changes on a background of normal skin. For these cases useful information may still be attainable with a model trained only on healthy examples. Furthermore, even if the segmentation approach is not directly applicable to a given lesion the underlying bag of features representation may be a useful starting point for designing automated tools, such as for melanoma detection in melanocytic lesions.

In conclusion, it has been shown that a bag of features model is an effective tool for automatically segmenting and analysing reflectance confocal microscopy depth stacks. The classifier accuracy appears sufficient for approximate segmentation of RCM depth stacks across all four identified strata. Furthermore, in the stratum corneum it may be sufficiently accurate to allow automatic measurement of stratum corneum thickness with accuracy similar to a dermatologist. Future studies will focus on improving classification accuracy in strata other than the stratum corneum as well as assessment of skin pathologies including neoplastic and inflammatory skin diseases such as actinic keratosis and psoriasis. Future work may also consider the use of statistical methods to interpret the automatically generated features as an additional means of deriving features for human examination of RCM sections.

Supporting Information

S1 Archive. The software implementation of the described method.
(ZIP)

S1 Fig. Algorithm flowcharts.
(PDF)

S1 Table. Classification results for all 5319 sections in the test set.
(CSV)

S2 Table. The classification results and interface locations for each stack in the test set.
(CSV)

S3 Table. Summary of stacks for each participant and location.
(CSV)

S4 Table. Summary of the number of en-face sections for each stack.
(CSV)

Author Contributions

Conceived and designed the experiments: SH TP MA AB HS. Performed the experiments: SH. Analyzed the data: SH MA AB TP. Wrote the paper: SH MA AB HS TP.

References

1. Rajadhyaksha M, Grossman M, Esterowitz D, Webb RH, Anderson RR. In Vivo Confocal Scanning Laser Microscopy of Human Skin: Melanin Provides Strong Contrast. *Journal of Investigative Dermatology*. 1995; 104: 946–952. doi: [10.1111/1523-1747.ep12606215](https://doi.org/10.1111/1523-1747.ep12606215) PMID: [7769264](https://pubmed.ncbi.nlm.nih.gov/7769264/)

2. Guitera P, Menzies SW, Longo C, Cesinaro AM, Scolyer RA, Pellacani G. In vivo confocal microscopy for diagnosis of melanoma and basal cell carcinoma using a two-step method: analysis of 710 consecutive clinically equivocal cases. *Journal of investigative dermatology*. 2012; 132: 2386–2394. Available: <http://www.nature.com/jid/journal/v132/n10/abs/jid2012172a.html> doi: [10.1038/jid.2012.172](https://doi.org/10.1038/jid.2012.172) PMID: [22718115](https://pubmed.ncbi.nlm.nih.gov/22718115/)
3. Gerger A, Koller S, Kern T, Massone C, Steiger K, Richtig E, et al. Diagnostic Applicability of In Vivo Confocal Laser Scanning Microscopy in Melanocytic Skin Tumors. *Journal of Investigative Dermatology*. 2005; 124: 493–498. doi: [10.1111/j.0022-202X.2004.23569.x](https://doi.org/10.1111/j.0022-202X.2004.23569.x) PMID: [15737188](https://pubmed.ncbi.nlm.nih.gov/15737188/)
4. Koller S, Gerger A, Ahlgrimm-Siess V, Weger W, Smolle J, Hofmann-Wellenhof R. In vivo reflectance confocal microscopy of erythematosquamous skin diseases. *Experimental Dermatology*. 2009; 18: 536–540. doi: [10.1111/j.1600-0625.2008.00822.x](https://doi.org/10.1111/j.1600-0625.2008.00822.x) PMID: [19320740](https://pubmed.ncbi.nlm.nih.gov/19320740/)
5. Gareau D. Automated identification of epidermal keratinocytes in reflectance confocal microscopy. *Journal of biomedical optics*. 2011; 16: 030502–030502. Available: <http://biomedicaloptics.spiedigitallibrary.org/article.aspx?articleid=1166725> doi: [10.1117/1.3552639](https://doi.org/10.1117/1.3552639) PMID: [21456857](https://pubmed.ncbi.nlm.nih.gov/21456857/)
6. Gareau D, Hennessy R, Wan E, Pellacani G, Jacques SL. Automated detection of malignant features in confocal microscopy on superficial spreading melanoma versus nevi. *Journal of biomedical optics*. 2010; 15: 061713–061713. Available: <http://biomedicaloptics.spiedigitallibrary.org/article.aspx?articleid=1103613> doi: [10.1117/1.3524301](https://doi.org/10.1117/1.3524301) PMID: [21198161](https://pubmed.ncbi.nlm.nih.gov/21198161/)
7. Raphael AP, Kelf TA, Wurm EMT, Zvyagin AV, Soyer HP, Prow TW. Computational characterization of reflectance confocal microscopy features reveals potential for automated photoageing assessment. *Experimental Dermatology*. 2013; 22: 458–463. doi: [10.1111/exd.12176](https://doi.org/10.1111/exd.12176) PMID: [23800056](https://pubmed.ncbi.nlm.nih.gov/23800056/)
8. Koller S, Wiltgen M, Ahlgrimm-Siess V, Weger W, Hofmann-Wellenhof R, Richtig E, et al. In vivo reflectance confocal microscopy: automated diagnostic image analysis of melanocytic skin tumours: Diagnostic image analysis of melanocytic skin tumours. *Journal of the European Academy of Dermatology and Venereology*. 2011; 25: 554–558. doi: [10.1111/j.1468-3083.2010.03834.x](https://doi.org/10.1111/j.1468-3083.2010.03834.x) PMID: [20735518](https://pubmed.ncbi.nlm.nih.gov/20735518/)
9. Kurugol S, Kose K, Park B, Dy JG, Brooks DH, Rajadhyaksha M. Automated Delineation of Dermal–Epidermal Junction in Reflectance Confocal Microscopy Image Stacks of Human Skin. *Journal of Investigative Dermatology*. 2014; doi: [10.1038/jid.2014.379](https://doi.org/10.1038/jid.2014.379)
10. Somoza E, Cula GO, Correa C, Hirsch JB. Automatic Localization of Skin Layers in Reflectance Confocal Microscopy. In: Campilho A, Kamel M, editors. *Image Analysis and Recognition*. Cham: Springer International Publishing; 2014. pp. 141–150. Available: http://link.springer.com/10.1007/978-3-319-11755-3_16
11. Wurm E, Longo C, Curchin C, Soyer H, Prow T, Pellacani G. In vivo assessment of chronological ageing and photoageing in forearm skin using reflectance confocal microscopy: Assessment of chronological ageing and photoageing using RCM. *British Journal of Dermatology*. 2012; 167: 270–279. doi: [10.1111/j.1365-2133.2012.10943.x](https://doi.org/10.1111/j.1365-2133.2012.10943.x) PMID: [22428802](https://pubmed.ncbi.nlm.nih.gov/22428802/)
12. Tamaki T, Yoshimuta J, Kawakami M, Raytchev B, Kaneda K, Yoshida S, et al. Computer-aided colorectal tumor classification in NBI endoscopy using local features. *Medical Image Analysis*. 2013; 17: 78–100. doi: [10.1016/j.media.2012.08.003](https://doi.org/10.1016/j.media.2012.08.003) PMID: [23085199](https://pubmed.ncbi.nlm.nih.gov/23085199/)
13. Avni U, Greenspan H, Konen E, Sharon M, Goldberger J. X-ray Categorization and Retrieval on the Organ and Pathology Level, Using Patch-Based Visual Words. *IEEE Transactions on Medical Imaging*. 2011; 30: 733–746. doi: [10.1109/TMI.2010.2095026](https://doi.org/10.1109/TMI.2010.2095026) PMID: [21118769](https://pubmed.ncbi.nlm.nih.gov/21118769/)
14. Caicedo JC, Cruz A, Gonzalez FA. Histopathology Image Classification Using Bag of Features and Kernel Functions. In: Combi C, Shahar Y, Abu-Hanna A, editors. *Artificial Intelligence in Medicine*. Springer Berlin Heidelberg; 2009. pp. 126–135. Available: http://link.springer.com/chapter/10.1007/978-3-642-02976-9_17
15. Nguyen MH, Torresani L, De La Torre F, Rother C. Weakly supervised discriminative localization and classification: a joint learning process. In *Computer Vision, 2009 IEEE 12th International Conference on*. IEEE; 2009. pp. 1925–1932. Available: http://ieeexplore.ieee.org/xpls/abs_all.jsp?arnumber=5459426
16. Puig S, Carrera C, Salerni G, Rocha-Portela J. Epidermis, Dermis and Epidermal Appendages. In: Hofmann-Wellenhof R, Pellacani G, Malvey J, Soyer HP, editors. *Reflectance Confocal Microscopy for Skin Diseases*. Berlin, Heidelberg: Springer Berlin Heidelberg; 2012. pp. 23–31. Available: http://link.springer.com/10.1007/978-3-642-21997-9_4
17. Hames S, Ardigò M, Soyer P, Bradley A, Prow T. Data from: automated segmentation of skin strata in reflectance confocal microscopy depth stacks. *dryad digital repository*. <http://dx.doi.org/10.5061/dryad.rg58m>; doi: [10.5061/dryad.rg58m](https://doi.org/10.5061/dryad.rg58m)
18. Coates A, Ng AY. Learning feature representations with k-means. In *Neural Networks: Tricks of the Trade*. Springer; 2012. pp. 561–580. Available: http://link.springer.com/chapter/10.1007/978-3-642-35289-8_30

19. Hyvärinen A, Hurri J, Hoyer PO. *Natural Image Statistics: A Probabilistic Approach to Early Computational Vision*. Springer Science & Business Media; 2009.
20. Dhillon IS, Modha DS. Concept Decompositions for Large Sparse Text Data Using Clustering. *Machine Learning*. 2001; 42: 143–175.
21. Nister D, Stewenius H. Scalable recognition with a vocabulary tree. In *Computer Vision and Pattern Recognition, 2006 IEEE Computer Society Conference on*. IEEE; 2006. pp. 2161–2168. Available: http://ieeexplore.ieee.org/xpls/abs_all.jsp?arnumber=1641018
22. Fulkerson B, Vedaldi A, Soatto S. Localizing Objects with Smart Dictionaries. In: Forsyth D, Torr P, Zisserman A, editors. *Computer Vision—ECCV 2008*. Springer Berlin Heidelberg; 2008. pp. 179–192. Available: http://link.springer.com/chapter/10.1007/978-3-540-88682-2_15
23. Krizhevsky A, Sutskever I, Hinton GE. ImageNet Classification with Deep Convolutional Neural Networks. In: Pereira F, Burges CJC, Bottou L, Weinberger KQ, editors. *Advances in Neural Information Processing Systems 25*. Curran Associates, Inc. 2012. pp. 1097–1105. Available: <http://papers.nips.cc/paper/4824-imagenet-classification-with-deep-convolutional-neural-networks.pdf>
24. Pedregosa F, Varoquaux G, Gramfort A, Michel V, Thirion B, Grisel O, et al. Scikit-learn: machine learning in Python. *Journal of Machine Learning Research*. 2011; 12: 2825–2830.
25. Ng AY. Feature Selection, L1 vs. L2 Regularization, and Rotational Invariance. In *Proceedings of the Twenty-first International Conference on Machine Learning*. New York, NY, USA: ACM; 2004. pp. 78. doi: [10.1145/1015330.1015435](https://doi.org/10.1145/1015330.1015435)
26. Hames S, Ardigò M, Soyer P, Bradley A, Prow T. Anatomical skin segmentation in reflectance confocal microscopy with weak labels. In *Digital image computing: techniques and applications (dICTA), 2015 international conference on*. 2015. p. In Press.